Journal of Computational and Applied Mathematics 436 (2024) 115320

Contents lists available at ScienceDirect

Journal of Computational and Applied Mathematics

journal homepage: www.elsevier.com/locate/cam

An adaptive element subdivision method based on the affine transformations and partitioning techniques for evaluating the weakly singular integrals

Baotao Chi [a,b], Zhichao Jia [a], Can Li [c], Qianjian Guo [a,*], Wei Yuan [a], Chuanming Ju [d]

[a] School of Mechanical Engineering, Shandong University of Technology, Zibo 255000, China
[b] Shandong Luoxiang Automobile Manufacturing Postdoctoral Research Institute, Linyi 276211, China
[c] Key Laboratory of Physical Oceanography, Ocean University of China, Qingdao 266100, China
[d] School of Electromechanical and Automotive Engineering, Yantai University, Yantai 264005, China

ARTICLE INFO

Article history:
Received 13 October 2022
Received in revised form 27 April 2023

Keywords:
Adaptive element subdivision
Weakly singular integrals
Domain partitioning technique
Affine transformation
Gaussian quadrature

ABSTRACT

In this paper, an adaptive element Subdivision Method based on the Affine transformations and Partitioning techniques (APSM) is presented for evaluating the weakly singular integrals with arbitrary shape of elements. The basic idea consists in partitioning the input surface element via affine transformation and then in generating a set of high-quality patches by adaptive binary-tree subdivision. The proposed method has some advantages over the conventional methods based on elements subdivision, i.e. the adaptive element subdivision, an improvement of the accuracy and a straight-forward implementation. By using the domain partitioning technique, the surface element can be divided into several element projection and subdivision regions under affine transformations. It is far more efficient to separately perform the element subdivision for different regions where the desirable patches are required. The ultimate patches in the vicinity of the singular point are calculated numerically by the coordinate transformation technique, while the remaining patches are evaluated accurately by the standard Gaussian quadrature. Several numerical examples are presented in order to validate the accuracy, efficiency and availability of the proposed method.

1. Introduction

Boundary element method (BEM) is an excellent and constructive computational technique for linear and exterior problems, as it exhibits the characteristics of superior accuracy and dimensionality reduction [1–5]. On account of the difficulty of evaluating the singular integrals, the application of the BEM to solve large-scale and complex engineering problems has yet to be improved to some extent, such as the crack problems [6], wave problems [7], elastodynamics [8], poroelastodynamics [9] and micro-electro-mechanical system resonators [10]. An essential consideration in the BEM community is ensuring that accurate and efficient evaluation of singular integrals can be achieved under any circumstances [11].

Since a crucial point for the success of the BEM is the careful numerical evaluation of the matrix entries, that must take place under the assumption that all the involved integrals are computed with a sufficiently high accuracy,

* Corresponding author.
E-mail address: guoqianjian@163.com (Q. Guo).

https://doi.org/10.1016/j.cam.2023.115320
0377-0427/

numerous integration techniques have been proposed and developed to eliminate the difficulties in dealing with the singular integrals, such as the analytical and semi-analytical methods [12], non-linear transformation methods [13], distance transformation methods [14] and adaptive element subdivision methods [15]. These integration approaches were born with the objective of eliminating part of the difficulties of the integral singularity in BEM, which have made significant achievements in the academic field and research applications. However, there was no escaping the fact that some drawbacks are generally associated with these methods.

Although analytical and semi-analytical methods were coupled successfully to the planar elements, the application of this method to solve problems with curved elements did have some limitations [16]. The non-linear transformation method is also an efficient technique, and yet it is tricky to provide a general and effective method for different surface elements. We are also grateful to Guiggiani for his excellent work in terms of singular integrals, which is extensively available due to its flexibility in dealing with various kernel functions [17]. The distance transformation method inherits all the merits of Guiggiani's outstanding contribution, which is a general approach to handling different orders of singularities. The main weakness of this approach is that more expansion terms in the integrand are pretty sensitive to the position of singular points in extreme circumstances [18].

In the efforts to significantly promote the performance of the evaluation of singular integrals, a number of integration methods have been proposed and made a substantial contribution to the research in this area, such as the Conventional Subdivision Method (CSM) [19], the Quad-Tree Subdivision Method (QTSM) [20], and the Spherical Subdivision Method (SSM) [21]. The main idea of these approaches is that each element can be subdivided into a set of sub-elements, and then the integration results can be calculated directly on the ultimate patches. Inevitably, there are some irregular or degenerate patches in the element subdivision of CSM. The quad-tree data structure is employed to improve the efficiency and robustness of QTSM. However, the QTSM produces excess patches for integration by the hierarchical data structure, which places an additional costly burden on the speed, reliability, and storage capabilities of the computer. To overcome all the difficulties concerning integral singularity, the SSM is proposed to divide the element into several sub-elements by a sequence of spheres. Note that the SSM involves a wide variety of templates available in the subdivision of an element, which could not properly be extended to the three-dimensional singular domain integrals for patch generation.

With the excellent attribute that the optimal binary tree data structure is flexible and convenient to be implemented, the Binary-Tree Subdivision Method (BTSM) [22,23] is proposed for evaluating the singular integrals with arbitrary shape of elements. However, the complexity of element projection cavity construction is the main barrier to implementing the BTSM algorithm, which is severely determined by the location of the singular point relative to the ultimate sub-elements. In particular, it should be noted that the ultimate sub-elements obtained by the BTSM or the QTSM are barely distributed along the radial direction. Based on the advantages of both the BTSM and SSM, an adaptive and efficient element Subdivision Method based on the Affine transformations and Partitioning techniques (APSM) is proposed for evaluating the singular integrals. Compared with the BTSM, it is unnecessary for the APSM to construct any projection cavity independently according to the relative locations of topological entities. The APSM is also invariably achievable and easy to implement for arbitrary elements subdivision without any templates in comparison with SSM.

The rest of the paper is organized as follows. Section 2 describes the main ideas of the adaptive element subdivision approach based on the domain partitioning technique. A detailed description of the binary-tree element subdivision scheme for different element subdivision regions is presented in Section 3. Section 4 introduces the basic implementation of geometry-adaptive projection polygon construction, and then the patch generation process of the given element projection region is demonstrated. Section 5 presents several numerical examples of arbitrary surface elements subdivision for evaluating the singular integrals, which demonstrates the accuracy, efficiency and availability of the proposed method. Section 6 concludes the paper with a summary and future work.

2. Element subdivision using domain partitioning technique

2.1. 3D affine transformations for partition

Based on the insight that arbitrary geometric models can be approximated by different types of sub-regions by various domain decomposition techniques, an adaptive and efficient element subdivision method based on the domain partitioning technique is presented. The proposed element subdivision method takes the following steps: preprocessing the initial domain partition, the element subdivision and projection regions construction, and ultimate high-quality patch generation. By the affine transformation techniques [24], the given surface element can be divided into several element subdivision regions and projection regions, respectively.

The affine transformation is an essential technique for solving spatial geometric problems, which consists of a linear transformation followed by a translation. As illustrated in Fig. 1, each affine transformation can be represented by a matrix that specifies the mapping between source and destination points for the transformation. A set of affine transformations can be mathematically expressed as a single overall transformation matrix. A cluster of scattered points belonging to an object also can be transformed into another group of points by any combination of linear transformations, such as translation, scaling, rotation, shear, etc. As has been demonstrated in Ref. [24], the fundamental theories of affine transformations have been well documented in mathematics. The 3D affine transformation is defined as

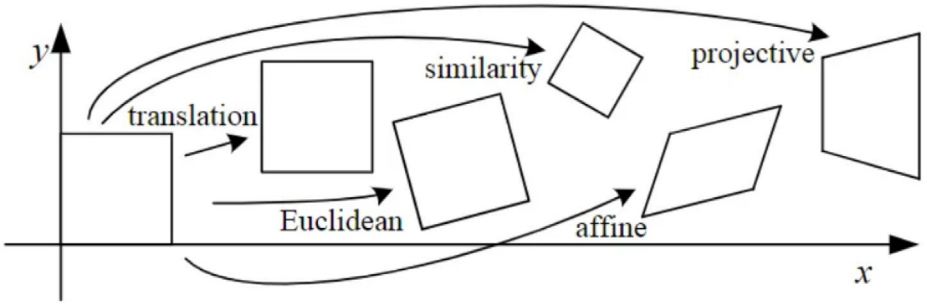

Fig. 1. Schematic of the 3D affine transformations.

Translation : $\mathbf{V}^* = \mathbf{D} \times \mathbf{V}$

$$\begin{bmatrix} x^* \\ y^* \\ z^* \\ 1 \end{bmatrix} = \begin{bmatrix} 1 & 0 & 0 & T_x \\ 0 & 1 & 0 & T_y \\ 0 & 0 & 1 & T_z \\ 0 & 0 & 0 & 1 \end{bmatrix} \begin{bmatrix} x \\ y \\ z \\ 1 \end{bmatrix} \tag{1}$$

Scaling : $\mathbf{V}^* = \mathbf{S} \times \mathbf{V}$

$$\begin{bmatrix} x^* \\ y^* \\ z^* \\ 1 \end{bmatrix} = \begin{bmatrix} S_x & 0 & 0 & 0 \\ 0 & S_y & 0 & 0 \\ 0 & 0 & S_z & 1 \\ 0 & 0 & 0 & 1 \end{bmatrix} \begin{bmatrix} x \\ y \\ z \\ 1 \end{bmatrix} \tag{2}$$

It is worth noting that a sequence of transformations can be represented by

$$\mathbf{T} = \mathbf{T}_1 \times \mathbf{T}_2 \times \cdots \times \mathbf{T}_N \tag{3}$$

where **D** and **S** are the translation and scaling matrices, respectively. **T** is the matrix transform. S_x, S_y, S_z are the scaling factors, (T_x, T_y, T_z) is the translation vectors. $\mathbf{V}^*(x^*, y^*, z^*, w)$ is the homogeneous coordinates of a point $\mathbf{V}(x, y, z)$ for any scale factor $w \neq 0$. More details of the 3D affine transformations can be available in [24].

2.2. Element projection region construction

To illustrate the APSM more clearly, the main ideas of the proposed method for evaluating the singular integrals are graphically illustrated in Fig. 2. Rather than directly constructing the element projection region, the 3D affine transformations are adopted to decompose the given element into several block-structured subdomains. Compared with the BTSM, the proposed method is more flexible and efficient for patch generation around the singular point without considering arbitrary projection cavity construction.

For a given surface element, the affine transformations and partitioning techniques can be available for constructing the element projection regions and subdivision regions under any circumstances. These purple boundary edges around the singular point in Fig. 2 are called the *projection cavity*. For volume elements subdivision using the APSM, the projection cavity will be composed of a group of triangular or quadrilateral facets. Based on the flexible configuration features and stable performance of the APSM, the dilemma of arbitrary element partition using 3D affine transformations can be avoidable.

A schematic description of the element projection region construction is depicted in Fig. 3. The scaling and translation transformations are incorporated to construct the bounding box of the singular point, and then the streamlines that emanate from these vertices of the bounding box are extracted according to the element shape. For a given surface element ABCD, the bounding box A'B'C'D' is constructed by the scaling transformation according to the scaling ratio η (see Fig. 3(b)). The scaling ratio η is defined as the ratio of the closest distance r to the maximum distance d from the singular point to the boundary of an element, i.e. $\eta = r/d$. After that, we can use the translation transformation to move

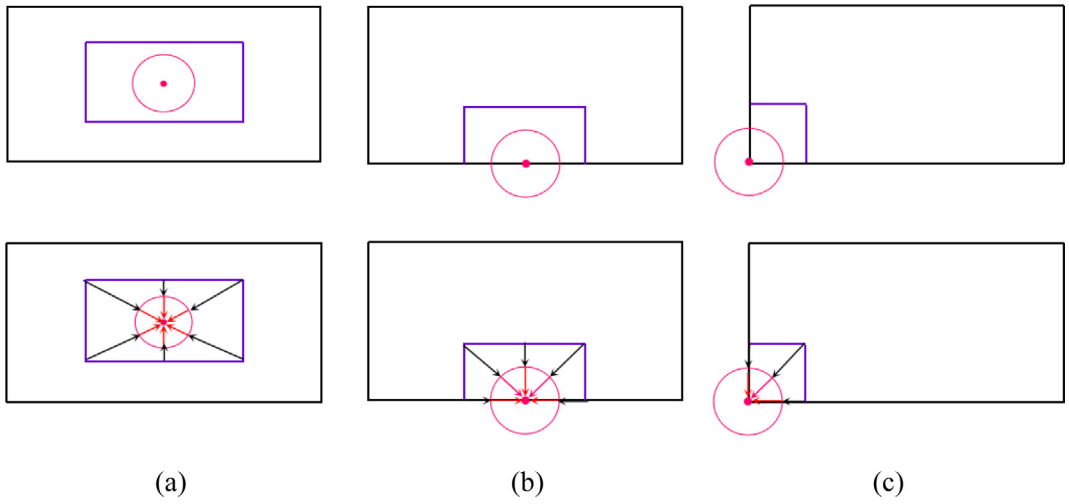

Fig. 2. Schematic of the APSM for arbitrary locations of the singular point: (a) inside, (b) on the boundary, and (c) at vertices.

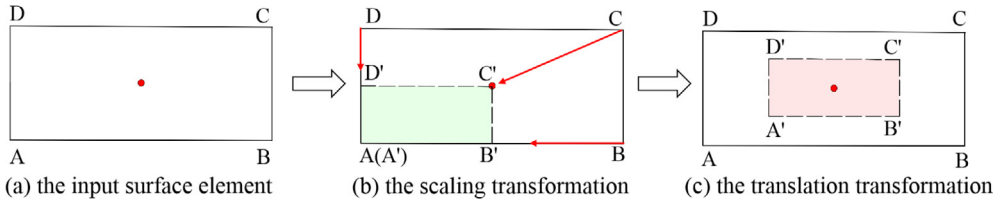

Fig. 3. Schematic of the element projection region construction.

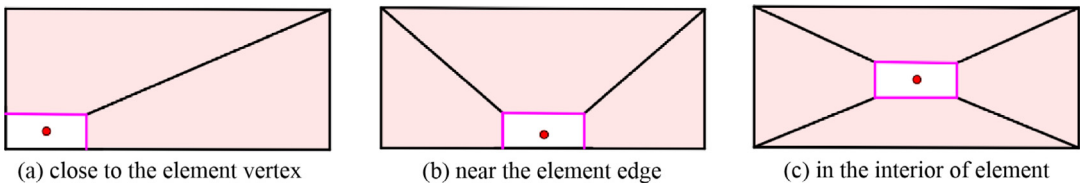

Fig. 4. The element projection region construction for different locations of the singular point.

the bounding box A'B'C'D' to the desired position in the vicinity of the singular point, as depicted in Fig. 3(c). Thus, a reasonable result of the element projection region can be achieved for different types of elements.

As is illustrated in Fig. 4, three different types of the element projection region construction templates have been identified based on the locations of the singular point: (i) close to the element vertex, (ii) near the element edge and (iii) inside the element. These element projection region construction templates can be classified into two categories. The first category indicates that the singular point is fairly close to the boundary of the element, including Type 1 and Type 2. Then, the element projection region is constructed by moving the bounding box to the element boundary. The second category has only one way of decomposition for the interior element projection region construction (see Type 3). These basic decomposition templates of an element are subdivided into a projection region and a few subdivision regions for an arbitrary singular point. It is appealing that a pair of opposite edges of the element projection region are parallel to each other, which is conducive to improving the quality of patch generation dramatically.

2.3. Element subdivision region construction

2.3.1. Notations for element partition

Aspect ratio: the width to the height of an element subdivision region. The aspect ratio of regular subdomains is approximately 1.0, while it generally means the irregular subdomain has an aspect ratio of 10:1 or larger for thin structures or sharp features.

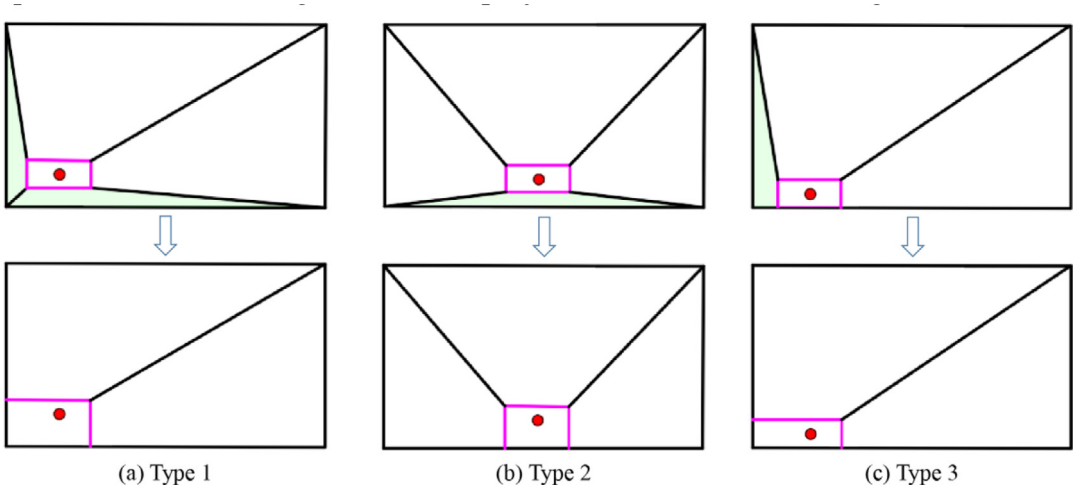

Fig. 5. Different types of decomposition templates for regular quadrilateral elements.

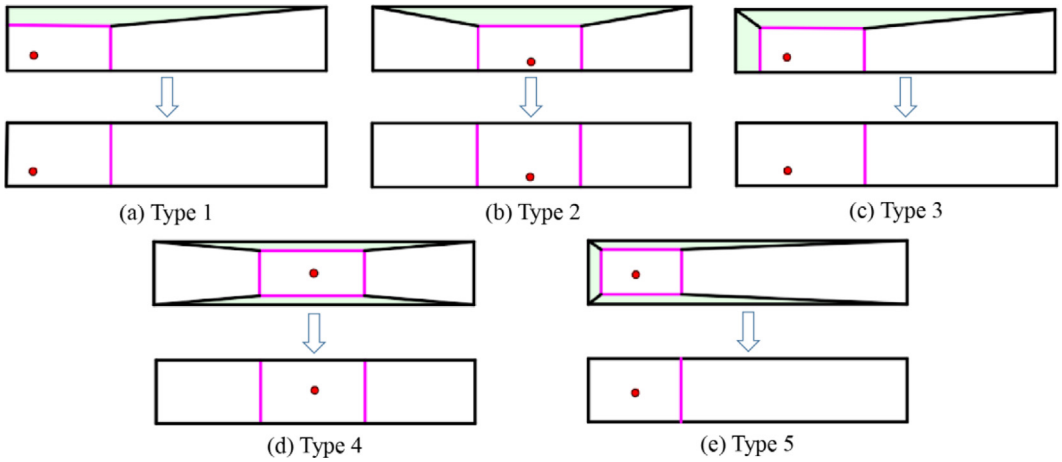

Fig. 6. Different types of decomposition templates for slender quadrilateral elements.

Parallel deviation: construct each pair of opposite unit vectors relative to the singular point, and take the arc cosine of the dot product of these vectors as the parallel deviation angle. If the parallel deviation angle exceeds 150°, the discrete subdomains are not acceptable for element subdivision.

Maximum corner angle: examine the maximum angle between adjacent segments of the singular point. For the regular triangular subdomains, the maximum corner angle is around 60°. The ultimate patch generation is not available for highly accurate numerical integration if a triangular subdomain contains an obtuse interior angle.

2.3.2. Decomposition templates for element partition

Due to the various locations of the singular point relative to the element, it is challenging directly to determine the element partition for arbitrary surface elements. There are a minority of unwanted subdomains by using the conventional element partitioning approach. Besides, adaptive elements subdivision and the density of the ultimate patch generation are required to be better controlled, and the number of decomposition templates may increase considerably. According to the initial position of the singular point, the domain partitioning procedures under 3D affine transformations are employed to construct the element projection and subdivision regions in this paper. Figs. 5 and 6 provide different types of decomposition templates for constructing the element projection and subdivision regions.

The decomposition templates for elements partition are defined by the element shape and the location of the singular point. Suppose the singular point is in the vicinity of the element vertex. In that case, the original surface element is decomposed into a projection region and two/one subdivision regions (Fig. 5(a), (c) and 6(a), (c), (e)). As illustrated in

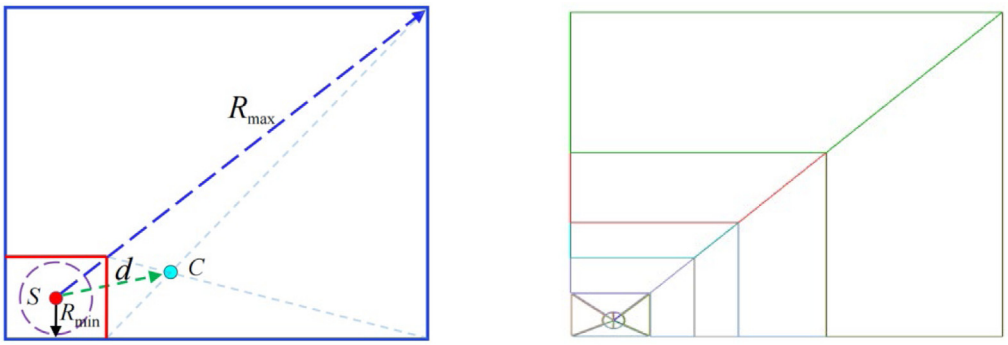

(a) The element subdivision criterion (b) The BTSM subdivision technique

Fig. 7. Schematic of the element subdivision criterion.

Fig. 5(b) and 6(b), (d), these decomposition templates depict that the singular point is adjacent to the boundary edge of a quadrilateral element, which is decomposed into a projection region and three/two subdivision regions. It should be noted that the decomposition templates for elements partition are not unique and can be developed under the specific requirements of element subdivision.

2.3.3. The element subdivision region construction algorithm

In order to create a reasonable and feasible element partition, the initial element partition must be pre-processed before the element subdivision. The primitive decomposition templates are employed to discretize the surface element into several block-structured subdomains. The procedures of the element subdivision region construction algorithm for elements partition are described in detail as follows (see Figs. 5 and 6):

(1) Identify the location of the singular point and construct the initial element projection region under 3D affine transformations;
(2) By directly connecting the element vertices and the points of a projection region, initial element subdivision regions can be constructed according to the fundamental decomposition templates in Fig. 4 in a purely sequential manner;
(3) Evaluate the element partition parameters illustrated in Section 2.3.1 of each subdivision region, and then mark the irregular element subdivision regions if these parameters are invalid;
(4) According to the initial element partition information, reconstruct the element projection and subdivision regions as the components of elements partition based on different decomposition templates automatically.

3. The binary-tree element refinement scheme

3.1. Element subdivision criterion

Combined with the domain partitioning technique, the input surface element can be well partitioned into a set of element projection and subdivision regions under affine transformations. It is more convenient and efficient to perform the element subdivision for different regions where the desirable patches are required. An eligible refinement structure for element subdivision regions should have a reasonable size or density distribution. In this section, a more specific implementation of the binary-tree refinement scheme for patch generation of the element subdivision regions is illustrated in detail.

Similar to other self-adapt spatial subdivision methods, the binary-tree refinement algorithm can provide more convenience for adaptive element subdivision for its validity and simplicity in practical application. The ultimate refinement structure is constructed according to the integral kernel function types and the surface element shapes. A schematic description of the refinement criterion for element subdivision is depicted in Fig. 7. To accurately and efficiently evaluate the singular integrals, the binary-tree element refinement criterion can be expressed as $d < R_{max}/2^i$. The geometric parameter d indicates the distance from the geometric center of each sub-element to the singular point. R_{min}, R_{max} represent the minimum and maximum distances between the singular point and the element boundary, respectively. The given surface element is subdivided into two children sub-elements, and each of them is then examined by the element subdivision criterion to determine whether to continue the binary-tree refinement scheme. With the excellent properties of simple self-adapt subdivision data structure, the binary-tree refinement technique is convenient and reliable to be applied in the APSM implementation.

3.2. Adaptive element subdivision based on BTSM

Due to the complexity of unstructured mesh generation, it is tricky to directly generate the refinement structure by a single binary-tree subdivision technique for arbitrary element subdivision regions. In order to accurately capture the geometric features of element subdivision regions, an adaptive generation technique based on BTSM [25] is employed to create the initial refinement structure. Based on the flexible configuration features and stable performance of BTSM, the element subdivision region is subdivided by the binary-tree refinement algorithm. This algorithm has the advantages of fast convergence speed, small number of convergences and not easy to get premature convergence. The number of iterations is determined by the location of the singular point and the order of singularity. In the APSM implementation process, the range of the maximum number of iterations is 4 to 6. In this way, the ultimate patch generation can completely extend the entire element subdivision regions. The binary-tree refinement algorithm for the adaptive element subdivision is carried out through the following techniques:

(1) Calculate the minimum and maximum distances $R_{\min}$, $R_{\max}$ relative to the given surface element.
(2) Execute the binary-tree refinement scheme for patch generation of all element subdivision regions according to the refinement criterion.
(3) To create high-quality and well-shaped patch generation, the element subdivision regions are preferentially subdivided into several children sub-elements along the radial direction.
(4) Determine whether the element subdivision ends with a prescribed value, and merge the smaller-sized sub-elements with their adjacent sub-elements to construct well-shaped patches.

4. Patch generation around the singular point

The desired refinement structure can be obtained for each element projection region through the binary-tree element subdivision scheme. Patch generation around the singular point is another indispensable part of adaptive element subdivision. In order to eliminate the singularity of integral kernels, the ultimate sub-elements in the element projection region are required to pass through the singular point. Several comprehensive techniques are applied to fill the void between the singular point and the boundary of the element projection region.

4.1. Geometry-adaptive projection polygon construction

Since different decomposition templates are adopted to construct the element projection and subdivision regions, generally, there is a relatively large distance between the boundary of the element projection region and the singular point. One of the basic requirements of patch generation is that the boundary of the projection region should be as near to the singular as possible. However, due to the uncertainty of the locations of the singular point, it is incredibly hard to generate high-quality patches by directly connecting the vertices of the element projection region and the singular point.

If the singular point locates in the vicinity of the center of the element projection region, well-shaped patches can be obtained by the direct approach. Provided that the singular point locates nearby the element vertices or edges, a self-adapt projection polygon construction scheme is adopted to deal with these tricky situations. By the affine transformation techniques and the binary-tree element refinement algorithms, the element projection region is decomposed into a number of sub-elements around the singular point. As is shown in Fig. 8, it is incredibly unique and acceptable that the ultimate sub-elements are automatically refined as they approach the singular point. The matching procedures are conducted by selecting the boundary of the sub-element adjacent to the singular point as the components of the projection polygon. To meet the requirement of high-accuracy singular integrals, optimum techniques by the curved boundary serendipity patches, i.e. the four-node triangular serendipity patches and the six-node quadrilateral serendipity patches, are employed to improve the quality of patch generation.

4.2. Patch generation of the element projection region

The refinement sub-elements outside the projection polygon are taken as the eligible patches for evaluating the singular integrals. To better characterize the integral kernels, the radial projection algorithm is incorporated to fill the void spaces around the singular point by inserting some sub-elements layer by layer through a sequence of spheres. The specific parameters of the spherical center and radius are determined by the singular point and the reference radius, respectively. The inserted new layer of triangular and quadrilateral sub-elements in the vicinity of the singular point is called the buffer layer, which can effectively improve the quality of ultimate patch generation rather than the single application of the direct method. Consider the problem of numerically evaluating the weakly singular integral of the form

$$I(P)=\int_{\Gamma} f(P,Q)N(Q)d\Gamma=\int_{\Gamma}\frac{f(P,Q)}{r(P,Q)}N(Q)d\Gamma \tag{4}$$

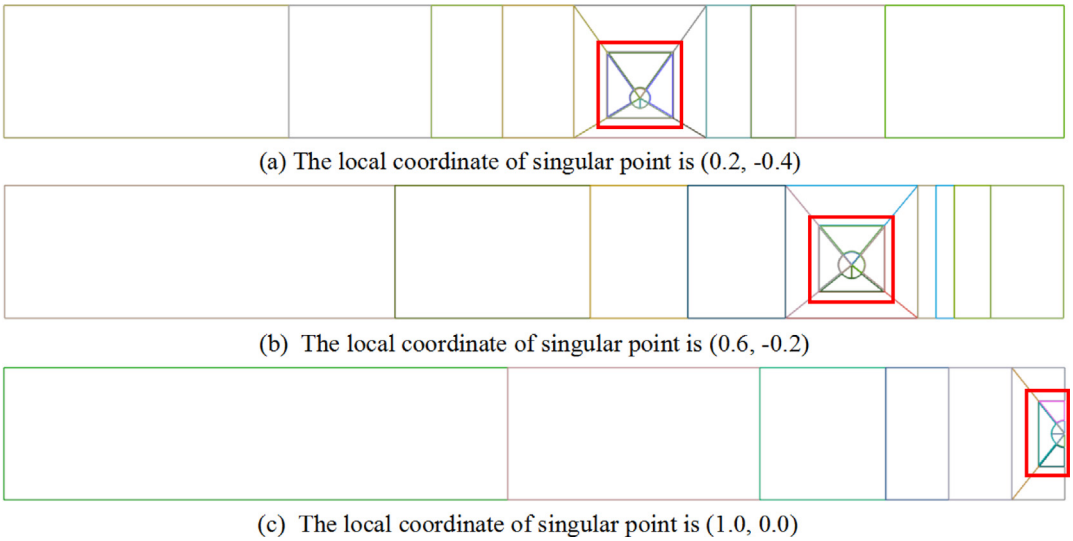

Fig. 8. Geometry-adaptive projection polygon construction and patch generation.

where *Gamma* is the domain of solving the given problem, *P* and *Q* represent the singular point and the field point, respectively, *r* is the distance from the singular point to the field point, f(P, Q) and N(Q) denote the integral kernel and the shape function, respectively.

In order to ensure that the sub-elements around the singular point are associated with the boundary of the spherical surface, the triangular and quadrilateral serendipity patches are adopted here for ultimate patch generation. Besides, a typical four-node triangular serendipity patch and a six-node quadrilateral serendipity patch are constructed for numerical integration. A more detailed explanation of these two types of serendipity patches will be described below. In addition to the serendipity patches around the singular point, the remaining regular patches are evaluated by conventional numerical quadrature with fewer integration points. As has been demonstrated numerically in Ref. [26–28], the number of integration points *m* is determined by

$$m = -\frac{1}{10}\ln\left(\frac{e}{2}\right)\sqrt{\frac{2}{3}p+\frac{2}{5}}\left[\left(\frac{8L}{3R}\right)^{\frac{3}{4}}+1\right] \tag{5}$$

where *e* is the integral error, *p* is the power of the exponent of the denominator in the kernel function, *L* indicates the length of a patch in the direction of integration, and *R* represents the minimum geometric distance from the singular point to the boundary of the given element.

4.2.1. The four-node triangular serendipity patch

For the four-node triangular serendipity patch, the coordinate transformation is applied to eliminate the singularities. As depicted in Fig. 9, all the nodes are located on the boundary of a triangular serendipity patch. Point 0 coincides with the singular point, and other points are located on the boundary of the spherical surface. Specifically, the coordinate transformation of a four-node triangular serendipity patch in terms of nodal coordinates, which can be expressed as

$$\begin{cases} x = x_0 + (x_a - x_0)\rho \\ y = y_0 + (y_a - y_0)\rho \end{cases} \quad \rho \in [0,\ 1] \tag{6}$$

Similarly, any point within the triangular serendipity patch is defined by

$$\begin{cases} x = x_0 + [(N_0 x_1 + N_2 x_3 + N_1 x_2) - x_0]\rho \\ y = y_0 + [(N_0 y_1 + N_2 y_3 + N_1 y_2) - y_0]\rho \end{cases} \tag{6a}$$

The generic shape functions can be defined along the quadratic curve 132 as

$$\begin{cases} N_0 = 0.5\theta(\theta - 1) \\ N_1 = 0.5\theta(\theta + 1) \\ N_2 = (1+\theta)(1-\theta) \end{cases} \quad \theta \in [-1,1] \tag{6b}$$

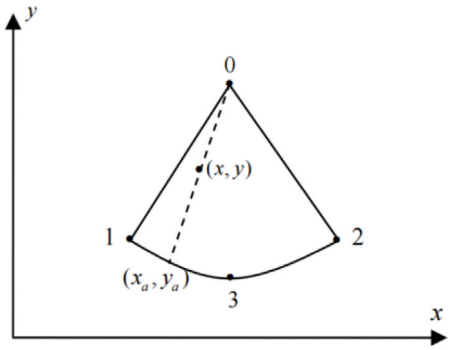

Fig. 9. The coordinate transformation of a four-node triangular serendipity patch.

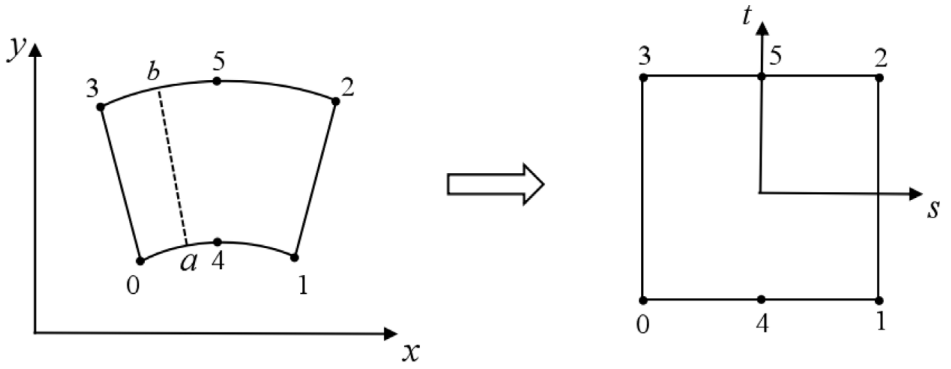

Fig. 10. The coordinate transformation of a six-node quadrilateral serendipity patch.

Thus, the evaluating singular integral of the form can be rewritten as

$$I(P)=\int_{-1}^{1}\int_{0}^{1}\frac{f(P,Q)}{r(P,Q)}N(Q)Jb(\rho,\theta)d\rho d\theta \tag{7}$$

where Jb(ρ, θ) is the Jacobian of the transformation from the *x*-*y* system to the $\rho-\theta$ system, which is given by

$$Jb=\rho\left[(x_a-x_0)\frac{\partial y_a}{\partial\theta}-(y_a-y_0)\frac{\partial x_a}{\partial\theta}\right] \tag{8}$$

4.2.2. The six-node quadrilateral serendipity patch

To better approximate the boundary of the spherical surface, the six-node quadrilateral serendipity patches are constructed in the implementation of APSM. The local node numbers for this type of serendipity patch are shown in Fig. 10(a). The square master patch is depicted in Fig. 10(b), i.e., $s\in[-1,\ 1]$, $t\in[-1,\ 1]$. These points of a quadrilateral serendipity patch are arranged in a counterclockwise direction. The quadratic curve 041 is located at the intersection of the given element and the spherical surface. Segments 03 and 12 are distributed along the radius direction. Specifically, the coordinate transformation of a six-node quadrilateral serendipity patch is given by

$$\begin{cases}x=\dfrac{1}{2}(1-t)x_a+\dfrac{1}{2}(1+t)x_b\\ y=\dfrac{1}{2}(1-t)y_a+\dfrac{1}{2}(1+t)y_b\end{cases} \tag{9}$$

where the points $(x_a, y_a), (x_b, y_b)$ located on the quadratic curves 041 and 352, respectively.

$$\begin{cases} x_a = N_0 x_0 + N_1 x_1 + N_2 x_4 \\ y_a = N_0 y_0 + N_1 y_1 + N_2 y_4 \end{cases} \tag{9a}$$

$$\begin{cases} x_b = N_0 x_3 + N_1 x_2 + N_2 x_5 \\ y_b = N_0 y_3 + N_1 y_2 + N_2 y_5 \end{cases} \tag{9b}$$

and the shape functions of Eqs. (9a) and (9b) can be written as

$$\begin{cases} N_0 = 0.5s(s-1) \\ N_1 = 0.5s(s+1) \\ N_2 = (1+s)(1-s) \end{cases} \tag{9c}$$

Subsequently, any point within the quadrilateral serendipity patch can be obtained by

$$\begin{cases} x = \sum_{i=0}^{5} L_i x_i \\ y = \sum_{i=0}^{5} L_i y_i \end{cases} \tag{9d}$$

where

$$\begin{aligned} &L_0 = -0.25s(1-s)(1-t) \quad L_1 = 0.25s(1+s)(1-t) \quad L_2 = 0.25s(1+s)(1+t) \\ &L_3 = -0.25s(1-s)(1+t) \quad L_4 = 0.5(1-s^2)(1-t) \quad L_5 = 0.5(1-s^2)(1+t) \end{aligned} \tag{9e}$$

Thus, the evaluating singular integral of the form can be rewritten as

$$I(P) = \int_{-1}^{1}\int_{-1}^{1} \frac{f(P,Q)}{r(P,Q)} N(Q) Jb(s,t) ds dt \tag{10}$$

By referring to the master patch in Fig. 10(b), the Jacobian transformation is given by

$$Jb = \begin{vmatrix} \frac{\partial x}{\partial s} & \frac{\partial y}{\partial s} \\ \frac{\partial x}{\partial t} & \frac{\partial y}{\partial t} \end{vmatrix} \tag{11}$$

By distributing the nodes along a quadratic curve, the triangular and quadrilateral serendipity patches are available to characterize the integral kernels sufficiently. Note that it is more convenient to implement for numerical integration in the local coordinate system by defining the range of local coordinates. Compared to the conventional integral patches, significantly better accuracy and higher efficiency can be promoted by the triangular and quadrilateral serendipity patches for singular integrals. More details of the triangular and quadrilateral serendipity patches can be available in [29].

5. Numerical examples

The accuracy and feasibility of the proposed method are verified for the evaluation of the singular integrals through several numerical examples. A comparison of the proposed method and conventional approaches for numerical integration is also given in this section. Several examples of arbitrary elements are employed to verify that the proposed method is satisfactory for practical purposes. In order to demonstrate the accuracy, efficiency, and availability of the APSM, the following weakly singular integral is considered

$$I = \int_{\Gamma} \frac{1}{4\pi r} N d\Gamma \tag{12}$$

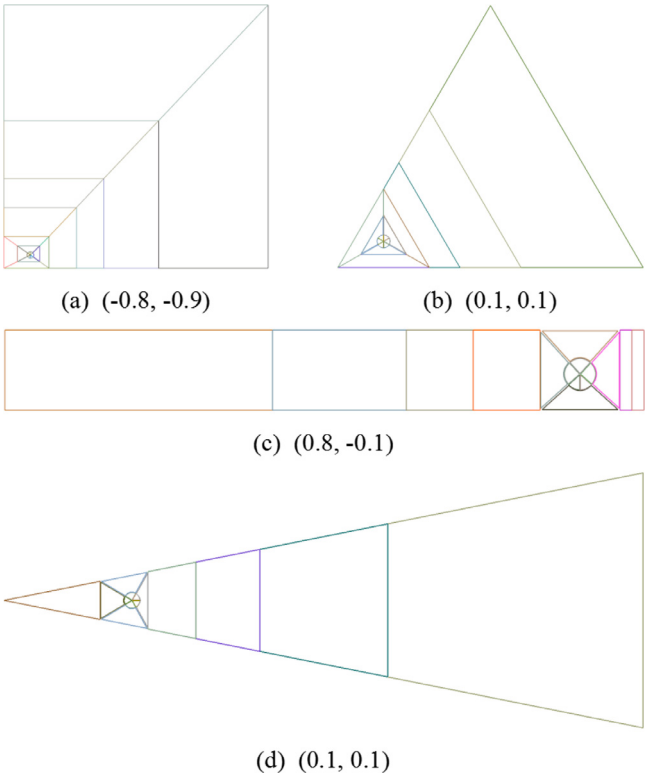

Fig. 11. Element subdivision for different types of elements by the APSM.

Relative errors are given to validate the accuracy and convergence of the APSM and other element subdivision methods, which are defined by

$$I_{err} = \left| \frac{I_n - I_e}{I_e} \right| \tag{13}$$

where Γ is the domain of integration, N is the shape functions of the given element, I_e and I_n represent the exact and numerical values of the singular integrals under consideration, respectively.

In order to obtain the exact value I_e for different types of elements, the prescribed element is subdivided into a large quantity of sub-elements and the integration points are set denser in each sub-element. Each sub-element is computed by the Gaussian quadrature [30] or the Hammer–Stroud quadrature [31]. Thus, numerical results obtained through the use of an enormous number of integration points can be taken as the reference result for comparison purposes.

Several examples are given to further demonstrate the accuracy, efficiency, and applicability of the proposed method. For demonstration purposes, the point coordinates of arbitrary shape of elements, the ultimate self-adapt element subdivision results and the number of integration points implemented by the APSM and other conventional methods based on elements subdivision are also investigated. The adaptive element subdivision results of arbitrary shape of elements with different locations of the singular points are illustrated in Figs. 11–18. A comparison of the accuracy and convergence performance of the APSM with the conventional methods based on elements subdivision for evaluating the weakly singular integrals is also given in Tables 1–7.

Unless otherwise mentioned, point coordinates of the linear regular quadrilateral element in Euclidean space are (0.0,0.0,0.0), (10.0,0.0,0.0), (10.0,10.0,0.0), (0.0,10.0,0.0). The point coordinates of the linear slender quadrilateral element are (0.0,0.0,0.0), (20.0,0.0,0.0), (20.0,2.5,0.0), (0.0,2.5,0.0), while the point coordinates of the linear irregular quadrilateral element are (0.0,0.0,0.0), (30.0,8.0,0.0), (13.0,15.0,0.0), (9.0,15.0,0.0). The point coordinates of the quadratic quadrilateral element are (0.0,0.0,0.0), (1.0,0.0,0.0), (1.0,1.0,0.0), (0.0,1.0,0.0), (0.5, −0.1, 0.0), (1.1,0.5,0.0), (0.5, 1.1, 0.0), (0.1, 0.5, 0.0). Point coordinates of the linear regular triangular element in Euclidean space are (0.0,0.0,0.0), (1.0,0.0,0.0), (1.0,1.0,0.0). The point coordinates of the linear slender triangular element are (0.0,1.0,0.0), (8.0,0.0,0.0), (8.0,2.0,0.0), while the point coordinates of the quadratic triangular element are (0.0,0.0,0.0), (1.0,0.0,0.0), (0.5,0.5,0.0), (0.5,0.05,0.0), (0.8,0.3,0.0), (0.2,0.3,0.0).

Table 1
Convergence of various element subdivision methods for different types of elements.

Element type	The location of source point	The number of the integration points			Relative error		
		CSM	BTSM	APSM	CSM	BTSM	APSM
Regular quadrilateral element	(−0.8, −0.9)	144	116	108	6.61e−02	1.89e−03	2.93e−04
		400	372	363	5.53e−03	4.03e−05	1.01e−06
		676	628	582	4.97e−04	3.35e−07	1.88e−08
Regular triangular element	(0.1, 0.1)	83	75	74	3.69e−02	5.72e−03	1.65e−04
		243	202	191	7.25e−03	3.29e−04	5.34e−05
		363	370	352	1.71e−03	3.72e−05	2.69e−06
Slender quadrilateral element	(0.8, −0.1)	100	95	92	4.87e−02	2.61e−03	5.91e−04
		256	224	213	1.28e−02	3.35e−05	2.06e−05
		484	429	412	9.35e−03	1.06e−06	1.32e−07
Slender triangular element	(0.1, 0.1)	83	78	72	6.37e−02	1.22e−03	7.51e−04
		300	293	278	5.62e−02	3.84e−04	1.86e−05
		363	371	358	2.49e−02	1.01e−05	3.52e−06

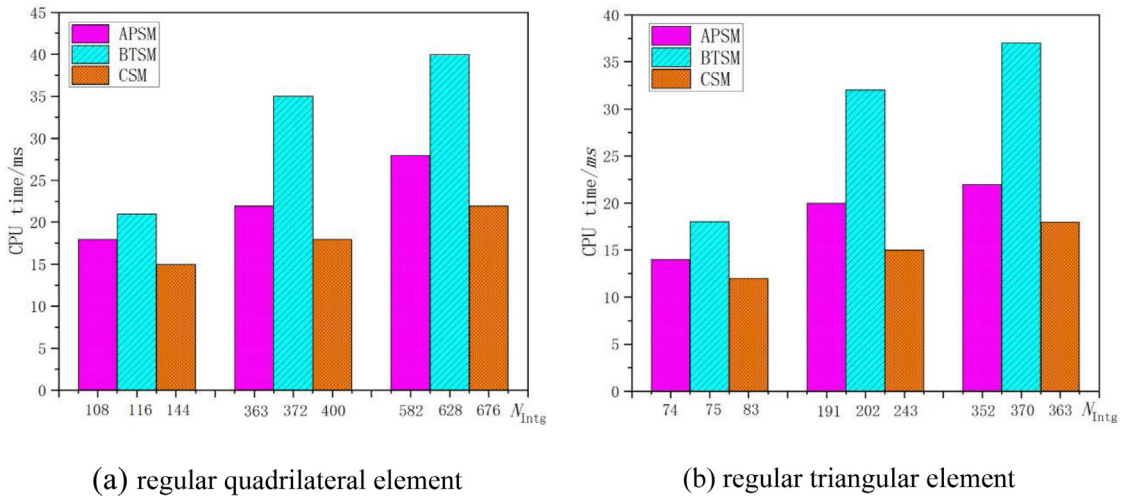

Fig. 12. Comparison of computational efficiency of different element subdivision methods.

5.1. Convergence performance of theAPSM

An adaptive element subdivision method based on the domain partitioning technique for evaluating the weakly singular integrals is presented. The first example is given to verify the effectiveness and convergence behavior of the proposed method. As is shown in Fig. 11, the element subdivision result for singular integrals is unique for the prescribed singular point. The computational efficiency of CSM, BTSM, and APSM is also investigated (see Fig. 12).

5.2. Evaluation of singular integrals for arbitrary elements

5.2.1. Slender triangular element

Fig. 13 depicts the adaptive element subdivision results of a slender triangular element with different locations of the singular point. The integration results of the APSM have been evaluated over four singular points randomly distributed from (0.0, 0.0) to (0.5, 0.5) in the local coordinate system.

5.2.2. Quadratic triangular element

Fig. 14 depicts the adaptive element subdivision results of a quadratic triangular element with different locations of the singular point. The integration results of the APSM have been evaluated over four singular points randomly distributed from (0.0, 0.0) to (0.5, 0.5) in the local coordinate system.

5.2.3. Regular quadrilateral element

Fig. 15 depicts the adaptive element subdivision results of a regular quadrilateral element with different locations of the singular point. The integration results of the APSM have been evaluated over six singular points randomly distributed from (−1.0, −1.0) to (1.0, 0.0) in the local coordinate system.

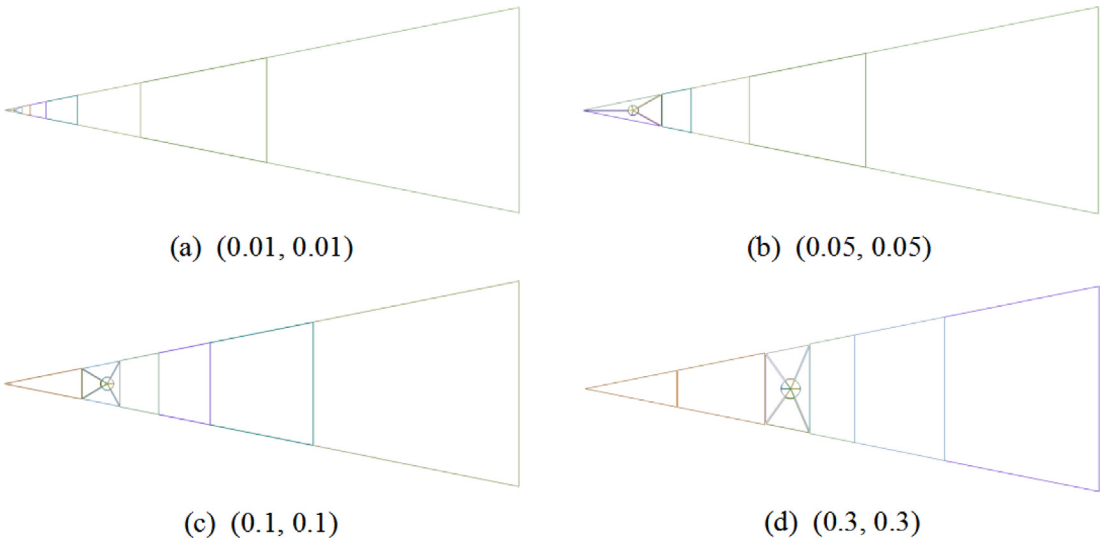

Fig. 13. Element subdivision for the linear triangular element by the APSM.

Table 2
Evaluation of singular integrals for the linear triangular element.

Element type	The location of source point	The number of the integration points			Relative error		
		CSM	BTSM	APSM	CSM	BTSM	APSM
Slender triangular element	(0.01, 0.01)	300	291	272	5.12e−02	3.41e−04	2.05e−05
	(0.05, 0.05)	300	296	286	4.15e−02	1.67e−04	1.53e−05
	(0.1, 0.1)	300	293	278	5.62e−02	3.84e−04	1.86e−05
	(0.3, 0.3)	363	372	331	2.93e−03	6.52e−05	2.90e−05

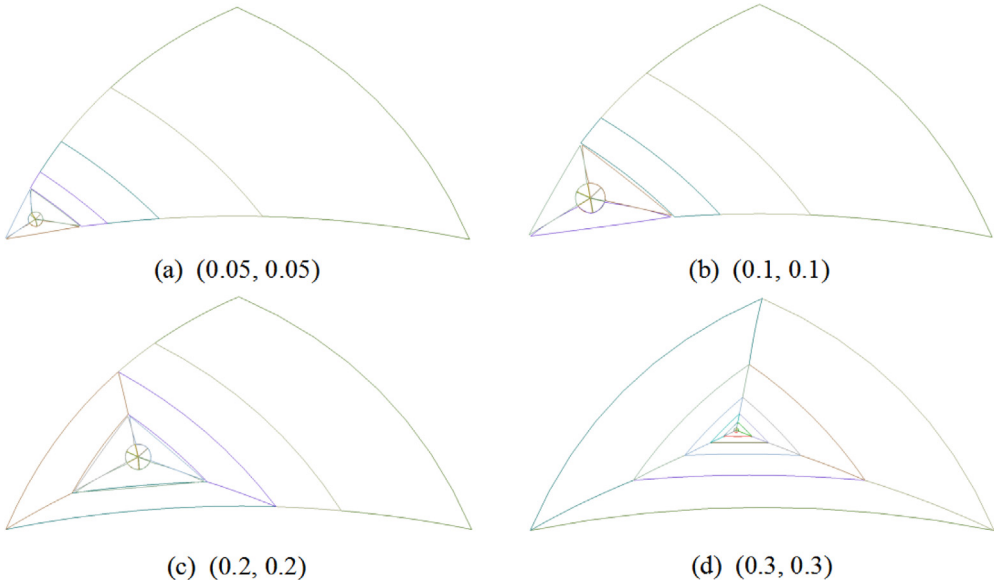

Fig. 14. Element subdivision for the quadratic triangular element by the APSM.

5.2.4. Slender quadrilateral element

Fig. 16 depicts the adaptive element subdivision results of a slender quadrilateral element with different locations of the singular point. The integration results of the APSM have been evaluated over six singular points randomly distributed from $(-1.0, -1.0)$ to $(1.0, 0.0)$ in the local coordinate system.

Table 3
Evaluation of singular integrals for the quadratic triangular element.

Element type	The location of source point	The number of the integration points			Relative error		
		CSM	BTSM	APSM	CSM	BTSM	APSM
Quadratic triangular element	(0.05, 0.05)	243	232	212	3.45e−03	7.32e−05	2.75e−05
	(0.1, 0.1)	243	221	191	7.25e−03	3.57e−05	5.34e−05
	(0.2, 0.2)	243	260	239	5.02e−03	5.76e−05	1.28e−05
	(0.3, 0.3)	363	352	328	6.89e−04	1.28e−05	3.09e−06

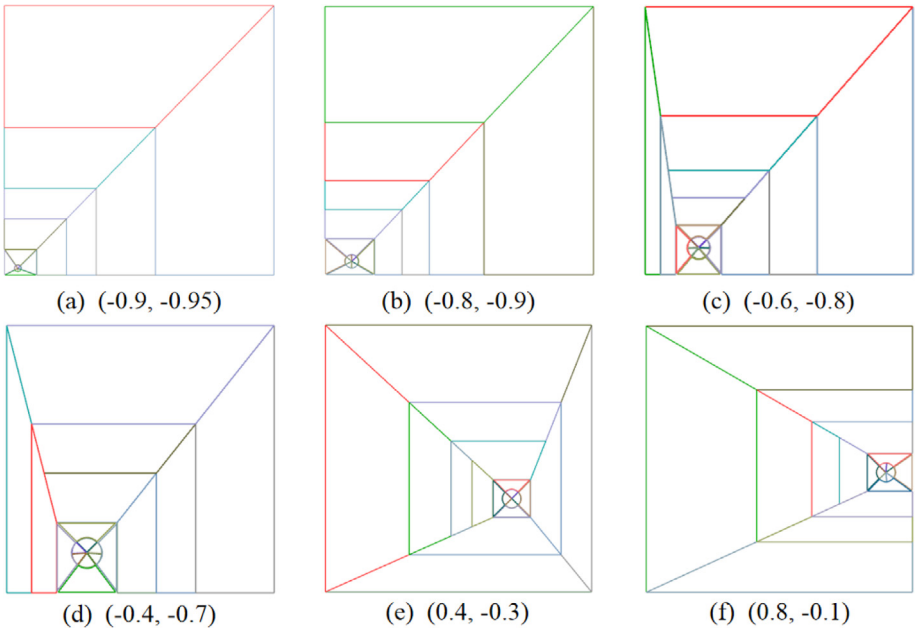

Fig. 15. Element subdivision for the regular quadrilateral element by the APSM.

Table 4
Evaluation of singular integrals for the regular quadrilateral element.

Element type	The location of source point	The number of the integration points			Relative error		
		CSM	BTSM	APSM	CSM	BTSM	APSM
Regular quadrilateral element	(−0.9, −0.95)	576	467	445	1.73e−03	3.37e−05	1.52e−06
	(−0.8, −0.9)	400	372	363	5.53e−03	4.03e−05	1.01e−06
	(−0.6, −0.8)	576	521	475	5.63e−04	1.29e−05	4.17e−06
	(−0.4, −0.7)	576	556	539	3.04e−03	2.36e−05	3.80e−06
	(0.4, −0.3)	484	489	462	5.32e−04	3.87e−06	2.57e−07
	(0.8, −0.1)	484	492	416	4.95e−04	6.07e−06	1.69e−07

Table 5
Evaluation of singular integrals for the slender quadrilateral element.

Element type	The location of source point	The number of the integration points			Relative error		
		CSM	BTSM	APSM	CSM	BTSM	APSM
Slender quadrilateral element	(−0.9, −0.95)	576	526	518	4.19e−02	3.95e−05	2.51e−06
	(−0.6, −0.8)	576	556	541	2.79e−02	3.37e−05	3.62e−06
	(−0.2, −0.6)	576	537	500	1.43e−02	5.08e−06	1.74e−06
	(0.2, −0.4)	576	522	460	1.45e−02	4.71e−06	2.08e−06
	(0.6, −0.2)	400	397	336	1.23e−02	3.99e−06	2.91e−06
	(0.9, −0.05)	324	317	272	1.43e−03	3.25e−05	1.50e−06

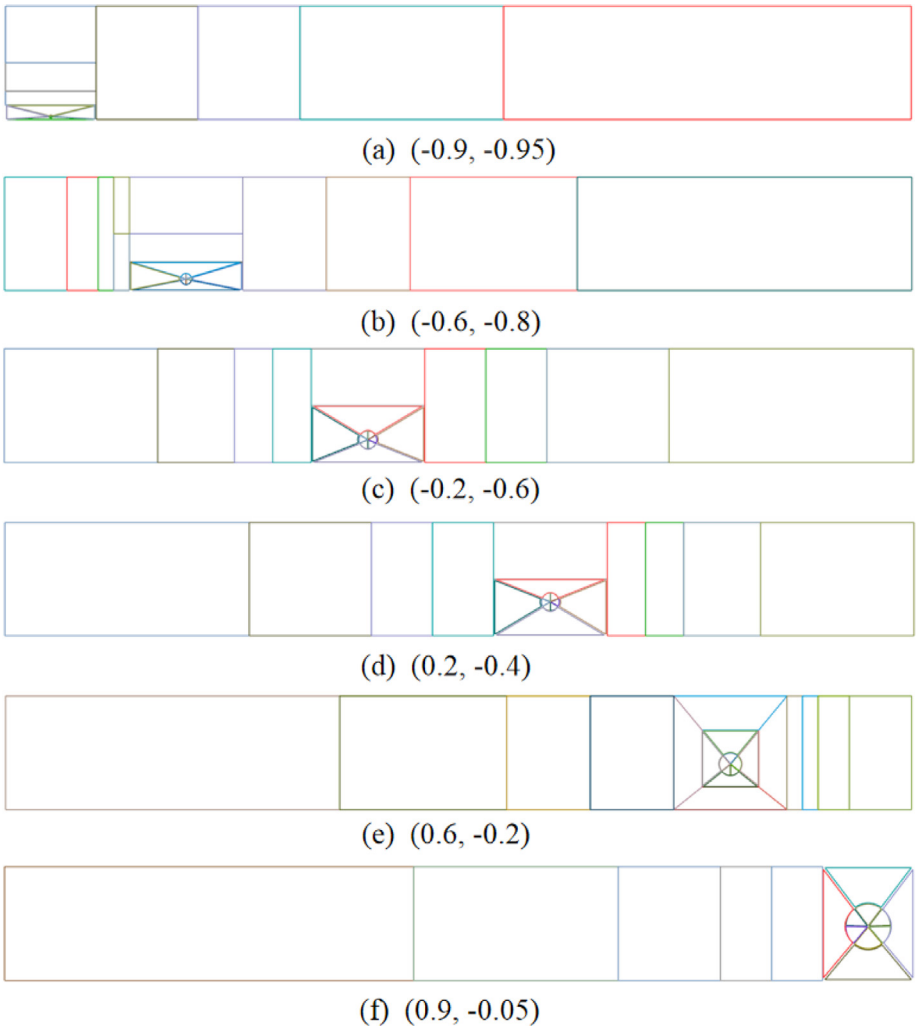

Fig. 16. Element subdivision for the slender quadrilateral element by the APSM.

Table 6
Evaluation of singular integrals for the irregular quadrilateral element.

Element type	The location of source point	The number of the integration points			Relative error		
		CSM	BTSM	APSM	CSM	BTSM	APSM
Irregular quadrilateral element	(−0.8, −0.9)	576	522	510	1.87e−02	3.26e−05	1.19e−06
	(−0.6, −0.8)	576	536	529	2.94e−03	1.12e−05	2.03e−06
	(−0.4, −0.7)	676	643	609	3.04e−03	6.15e−06	3.80e−06
	(−0.2, −0.6)	676	658	635	3.59e−03	3.39e−06	1.27e−06
	(0.0, −0.5)	676	637	620	2.68e−03	1.85e−06	1.21e−07
	(0.8, −0.1)	676	643	617	5.26e−03	2.93e−06	2.61e−07

5.2.5. Irregular quadrilateral element

Fig. 17 depicts the adaptive element subdivision results of a irregular quadrilateral element with different locations of the singular point. The integration results of the APSM have been evaluated over six singular points randomly distributed from (−1.0, −1.0) to (1.0, 0.0) in the local coordinate system.

5.2.6. Quadratic quadrilateral element

Fig. 18 depicts the adaptive element subdivision results of a irregular quadrilateral element with different locations of the singular point. The integration results of the APSM have been evaluated over six singular points randomly distributed from (−1.0, −1.0) to (1.0, 0.0) in the local coordinate system.

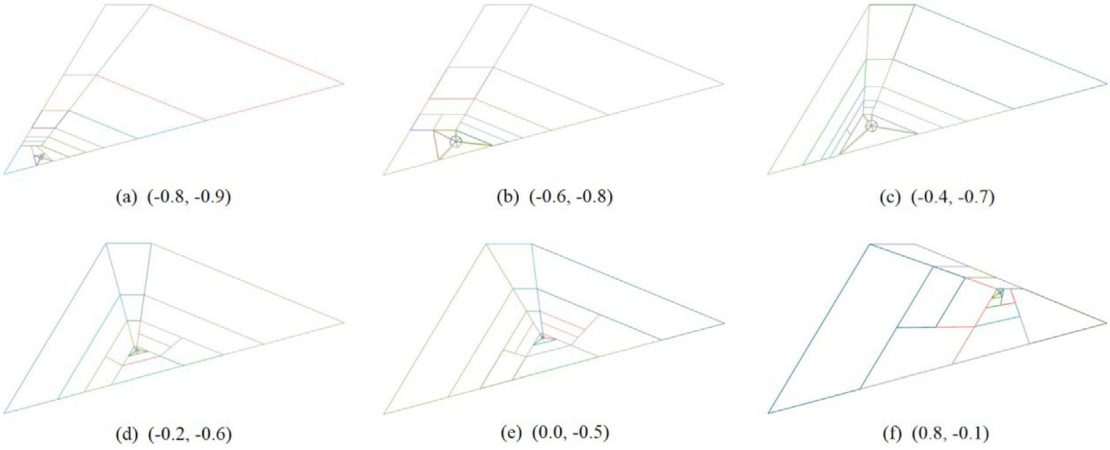

Fig. 17. Element subdivision for the irregular quadrilateral element by the APSM.

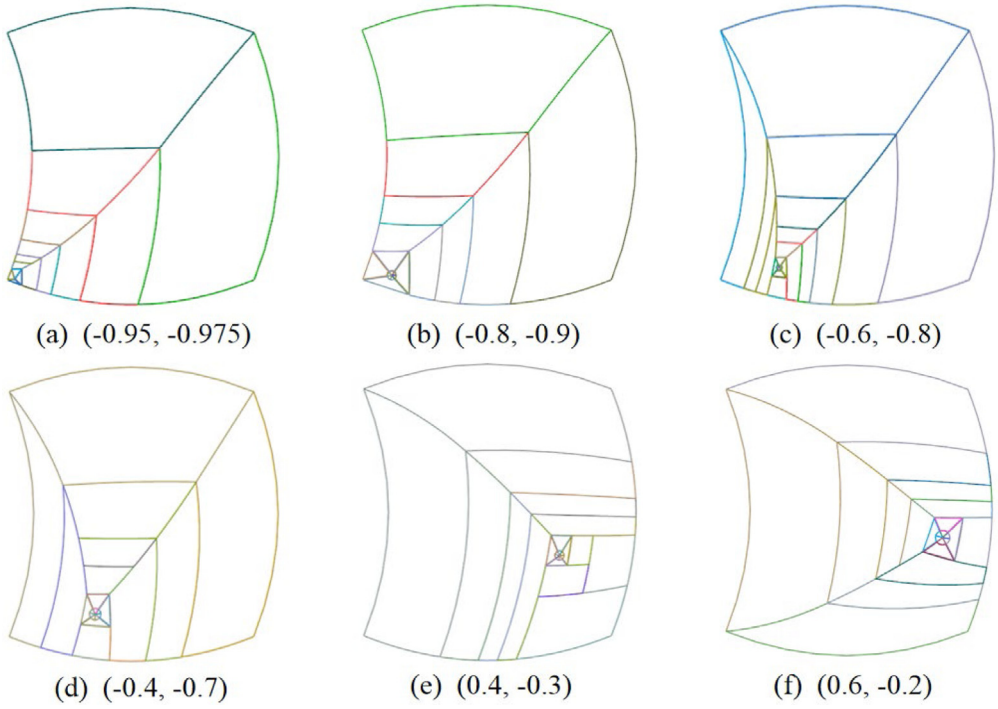

Fig. 18. Element subdivision for the quadratic quadrilateral element by the APSM.

As illustrated in Figs. 11–18, the accuracy and convergence performance of the APSM are significantly promoted with the increasing number of integration points in comparison with the conventional methods based on elements subdivision. According to the relative errors of numerical results, the accuracy and convergence of the APSM are superior to the conventional methods based on elements subdivision under almost the same number of integration points. As can be seen from Fig. 12, the APSM requires less CPU and memory allocation than the BTSM for the same level of integration accuracy. It is also appealing that high-quality patch generation can be achieved by the APSM, which is flexible and satisfactory for arbitrary elements subdivision with different locations of singular points.

6. Conclusions

The paper presents an adaptive subdivision method based on the affine transformations and partitioning techniques, for evaluating the weakly singular integrals with arbitrary shape of elements. With the APSM, an arbitrary element can be

Table 7
Evaluation of singular integrals for the quadratic quadrilateral element.

Element type	The location of source point	The number of the integration points			Relative error		
		CSM	BTSM	APSM	CSM	BTSM	APSM
Irregular quadrilateral element	(−0.95, −0.975)	576	561	519	1.53e−03	3.35e−05	2.61e−06
	(−0.8, −0.9)	576	537	526	5.99e−03	6.29e−05	1.29e−06
	(−0.6, −0.8)	576	572	558	5.63e−04	4.52e−06	2.08e−06
	(−0.4, −0.7)	576	565	509	3.04e−03	5.52e−06	3.80e−06
	(0.4, −0.3)	576	541	532	5.32e−05	1.55e−06	3.58e−07
	(0.6, −0.2)	576	526	467	6.54e−05	2.75e−06	1.69e−07

decomposed into the element projection and subdivision regions under affine transformation. By the domain partitioning techniques and the binary-tree subdivision algorithms, the ultimate patches are automatically refined as they approach the singular point. The integration points are set denser around the singular point, and are sparsely distributed away from it. The APSM is applicable to evaluate the singular integrals with arbitrary shape of elements and various locations of the singular point.

A comparison of the APSM with the conventional methods based on elements subdivision illustrates its competitiveness and wide applicability for evaluating the singular integrals. Even with some irregular elements in numerical integration, significantly better accuracy and higher efficiency can be promoted by the proposed method. Several numerical results demonstrate that the proposed method has some obvious advantages over other conventional methods based on elements subdivision, i.e. the adaptive element subdivision, an improvement of the accuracy, and a straight-forward implementation. Based on excellent properties of spline rules for integration [32–35], an extension of this work for hypersingular integrals can be observed in future work.

Data availability

Data will be made available on request

Acknowledgments

This work was supported by the National Natural Science Foundation of China (12202251, 12172201, 51805299), Project funded by China Postdoctoral Science Foundation (2021M702024, 2022M712393), Ministry of Education Industry-school Cooperative Education Project (220606517023742), the Key Research and Development Project of Shandong Province (2019GGX104081, 2019GGX104033), Zibo City School-City Integration Project (2018ZBXC265), the Shandong Provincial Natural Science Foundation, China (ZR2022ME122, ZR2022QA072), the Scientific Research Project of Shandong University of Technology (4041/420047, 4003/122237, 9101/2222431), Shandong Province's Key Support Regions Introducing Urgently Needed Talent Projects, and Young Innovative Talents Introduction and Training Program Project of Shandong Provincial Department of Education.

References

[1] J.M. Zhang, B.T. Chi, W.C. Lin, et al., A dual interpolation boundary face method for three-dimensional potential problems, Int. J. Heat Mass Transfer 140 (2019) 862–876.
[2] G.Z. Xie, Y.D. Zhong, F.L. Zhou, et al., Singularity cancellation method for time-domain boundary element formulation of elastodynamics: A direct approach, Appl. Math. Model. 80 (2019) 647–667.
[3] F. Zhou, J. Zhang, X. Sheng, et al., Shape variable radial basis function and its application in dual reciprocity boundary face method, Eng. Anal. Bound. Elem. 35 (2) (2011) 244–252.
[4] M. Schanz, Application of 3D time domain boundary element formulation to wave propagation in poroelastic solids, Eng. Anal. Bound. Elem. 25 (4/5) (2001) 363–376.
[5] S. Falletta, BEM coupling with the FEM fictitious domain approach for the solution of the exterior Poisson problem and of wave scattering by rotating rigid bodies, IMA J. Numer. Anal. 38 (2) (2018) 779–809.
[6] G.Z. Xie, F.L. Zhou, D.H. Zhang, et al., A novel triangular boundary crack front element for 3D crack problems based on 8-node serendipity element, Eng. Anal. Bound. Elem. 105 (2019) 296–302.
[7] L. Desiderio, S. Falletta, Efficient solution of two-dimensional wave propagation problems by CQ-wavelet BEM: Algorithm and applications, SIAM J. Sci. Comput. 2020 (4) 894–920.
[8] L. Desiderio, An H-matrix based direct solver for the boundary element method in 3D elastodynamics, in: AIP Conference Proceedings, 1978, p. 120005.
[9] M. Schanz, Fast multipole method for poroelastodynamics, Eng. Anal. Bound. Elem. 89 (2018) 50–59.
[10] A. Aimi, L. Desiderio, P. Fedeli, et al., A fast boundary-finite element approach for estimating anchor losses in micro-electro-mechanical system resonators, Appl. Math. Model. 97 (2021) 741–753.
[11] X.W. Gao, K. Yang, J. Wang, An adaptive element subdivision technique for evaluation of various 2D singular boundary integrals, Eng. Anal. Bound. Elem. 32 (8) (2008) 692–696.

[12] Z. Hu, Z. Niu, C. Cheng, A new semi-analytic algorithm of nearly singular integrals on higher order element in 3D potential BEM, Eng. Anal. Bound. Elem. 63 (2016) 30–39.
[13] J.C.F. Telles, A self-adaptive co-ordinate transformation for efficient numerical evaluation of general boundary element integrals, Internat. J. Numer. Methods Engrg. 24 (5) (1987) 959–973.
[14] H. Ma, N. Kamiya, A general algorithm for the numerical evaluation of nearly singular boundary integrals of various orders for two-and three-dimensional elasticity, Comput. Mech. 29 (4) (2002) 277–288.
[15] M.H. Aliabadi, D. Martin, Boundary element hyper-singular formulation for elastoplastic contact problems, Internat. J. Numer. Methods Engrg. 48 (7) (2000) 995–1014.
[16] G. Karami, D. Derakhshan, An efficient method to evaluate hypersingular and supersingular integrals in boundary integral equations analysis, Eng. Anal. Bound. Elem. 23 (4) (1999) 317–326.
[17] M. Guiggiani, G. Krishnasamy, T.J. Rudolphi, et al., A general algorithm for the numerical solution of hypersingular boundary integral equations, J. Appl. Mech. 59 (1992) 604–614.
[18] M. Guiggiani, P. Casalini, Direct computation of Cauchy principal value integrals in advanced boundary elements, Internat. J. Numer. Methods Engrg. 24 (9) (1987) 1711–1720.
[19] R. Klees, Numerical calculation of weakly singular surface integrals, J. Geod. 70 (11) (1996) 781–797.
[20] M. Tanaka, J.M. Zhang, T. Matsumoto, Boundary-type meshless solution of potential problems: Comparison between singular and regular formulations in hybrid BNM transactions of JASCOME, J. Bound. Elem. Methods 20 (2003) 21–26.
[21] J.M. Zhang, C. Lu, X. Zhang, et al., An adaptive element subdivision method for evaluation of weakly singular integrals in 3D BEM, Eng. Anal. Bound. Elem. 51 (2015) 213–219.
[22] B.T. Chi, Q. Guo, L. Zhang, et al., An adaptive binary-tree element subdivision method for evaluation of volume integrals with continuous or discontinuous kernels, Eng. Anal. Bound. Elem. 134 (2022) 298–314.
[23] J.M. Zhang, B.T. Chi, K.M. Singh, et al., A binary-tree element subdivision method for evaluation of singular domain integrals with continuous or discontinuous kernel, Eng. Anal. Bound. Elem. 116 (2020) 14–30.
[24] B. Margrit, C.M. Nicholas, Recognition, resolution, and complexity of objects subject to affine transformations, Int. J. Comput. Vis. 44 (1) (2001) 5–40.
[25] J.M. Zhang, B.T. Chi, K.M. Singh, et al., A binary-tree element subdivision method for evaluation of nearly singular domain integrals with continuous or discontinuous kernel, J. Comput. Appl. Math. 362 (2019) 22–40.
[26] X.W. Gao, T.G. Davies, Adaptive integration in elasto-plastic boundary element analysis, J. Chin. Inst. Eng. 23 (3) (2000) 349–356.
[27] S. Bu, T.G. Davies, Effective evaluation of non-singular integrals in 3D BEM, Adv. Eng. Softw. 23 (2) (1995) 121–128.
[28] J.C. Lachat, J.O. Watson, Effective numerical treatment of boundary integral equations: A formulation for three-dimensional elastostatics, Internat. J. Numer. Methods Engrg. 10 (5) (1976) 991–1005.
[29] Y. Zhong, J. Zhang, Y. Dong, et al., A serendipity triangular patch for evaluating weakly singular boundary integrals, Eng. Anal. Bound. Elem. 69 (2016) 86–92.
[30] J. Kosinka, M. Barton, Gaussian quadrature for C1 cubic Clough–Tocher macro-triangles, J. Comput. Appl. Math. 351 (2019) 6–13.
[31] P.C. Hammer, A.H. Stroud, Numerical integration over simplexes, Math. Tables Other Aids Comput. 10 (55) (1956) 137–139.
[32] M. Barton, V.M. Calo, Optimal quadrature rules for odd-degree spline spaces and their application to tensor-product-based isogeometric analysis, Comput. Methods Appl. Mech. Engrg. 305 (2016) 217–240.
[33] K. Johannessen, Optimal quadrature for univariate and tensor product splines, Comput. Methods Appl. Mech. Engrg. 316 (2017) 84–99.
[34] M. Barton, V.M. Calo, Gauss-Galerkin quadrature rules for quadratic and cubic spline spaces and their application to isogeometric analysis, Comput. Aided Des. 82 (2017) 57–67.
[35] A. Aimi, F. Calabrò, A. Falini, et al., Quadrature formulas based on spline quasi-interpolation for hypersingular integrals arising in IgA-SGBEM, Comput. Methods Appl. Mech. Engrg. 372 (2020) 113441.